Journal of Power Sources 248 (2014) 1067–1076

Contents lists available at ScienceDirect

Journal of Power Sources

journal homepage: www.elsevier.com/locate/jpowsour

Effects of using $(La_{0.8}Sr_{0.2})_{0.95}Fe_{0.6}Mn_{0.3}Co_{0.1}O_3$ (LSFMC), $LaNi_{0.6}Fe_{0.4}O_{3-\delta}$ (LNF) and $LaNi_{0.6}Co_{0.4}O_{3-\delta}$ (LNC) as contact materials on solid oxide fuel cells

Aroa Morán-Ruiz [a], Karmele Vidal [a], Miguel Ángel Laguna-Bercero [b], Aitor Larrañaga [a,*], María Isabel Arriortua [a,*]

[a] Universidad del País Vasco (UPV/EHU), Facultad de Ciencia y Tecnología, Departamento de Mineralogía y Petrología, Barrio Sarriena S/N, 48940 Leioa, Vizcaya, Spain
[b] Instituto de Ciencia de Materiales de Aragón, ICMA, CSIC-Universidad de Zaragoza, Pedro Cerbuna 12, 50009 Zaragoza, Spain

HIGHLIGHTS

- Lanthanum-based perovskite ceramic contact materials were studied.
- Contact resistance of $La_{0.6}Sr_{0.4}FeO_3$/contact layer/Crofer22APU is evaluated.
- Contact resistance of contact materials studied depends on their conductivity.

ARTICLE INFO

Article history:
Received 12 July 2013
Received in revised form
23 September 2013
Accepted 2 October 2013
Available online 23 October 2013

Keywords:
SOFC
Interconnect
Contact perovskite
Ohmic resistance losses
Electrical contact

ABSTRACT

Three lanthanum-based perovskite ceramic compounds were studied as contact materials, $(La_{0.8}Sr_{0.2})_{0.95}Fe_{0.6}Mn_{0.3}Co_{0.1}O_3$ (LSFMC), $LaNi_{0.6}Fe_{0.4}O_{3-\delta}$ (LNF) and $LaNi_{0.6}Co_{0.4}O_{3-\delta}$ (LNC), between a Crofer22APU interconnect and a $La_{0.6}Sr_{0.4}FeO_3$ (LSF) cathode. The layers were deposited using in all cases wet colloidal spray technique. Phase structures of materials were checked by X-ray Diffraction (XRD) measurements. Electrical conductivity and thermal expansion coefficient (TEC) for these selected compounds were also determined.

The important properties of the resulting {interconnect/contact layer/cathode} systems; including area specific resistance (ASR), reactivity, and adhesion of contact materials to the interconnect and to the cathode were investigated. Moreover, the electrical resistance and reactivity of the system without a contact layer, {steel/LSF/LSF} system, was measured for comparison. The contact resistance is strongly influenced by the conductivity of selected contact materials, showing the lowest ASR values for {Crofer22APU/LNC/LSF} assembly. The point microanalysis on cross-section of the systems, after ASR measurements, reveals that there is chromium enrichment in the contact and cathode layers which allows the formation of phases like $SrCrO_4$ and Cr-containing perovskite in short exposure times. An adequate integrity and low reactivity is achieved when LNF contact coating is applied between Crofer22APU and LSF cathode without compromising the contact resistance of the system.

1. Introduction

Despite IT-SOFCs advantages, lacks of contact between interconnect ribs and electrode is still unsolved. The interfacial adhesion between the oxide scale and electrode is very important for the durability of the cell [1]. To solve this problem, cathode contact layers are used between interconnect an electrode, and is often accomplished by compression of the stack using and external load frame [2,3]. In practice, however, adhesion between contact material/interconnect needs even to be improved. Cathode contact materials, apart from providing electrical contact between adjacent components, can also serve to improve in-plane conduction over the area of the cathode. In this case, contact material acts as a layer of the electrocatalyst used in the cathode [4,5].

Earlier studies have concluded that the use of cathode contact layers improves electrons transfer through the contact interface from interconnect to activate cathode layer [6]. Therefore, the

* Corresponding authors. Tel.: +34 946012534, +34 946015984.
E-mail addresses: aitor.larranaga@ehu.es (A. Larrañaga), maribel.arriortua@ehu.es (M.I. Arriortua).

0378-7753/$ – see front matter © 2013 Elsevier B.V. All rights reserved.
http://dx.doi.org/10.1016/j.jpowsour.2013.10.031

Table 1
Sintering procedure used for fabrication of rectangular bars for electrical conductivity and the degree of compaction (%) obtained for each material.

Composition	Sintering procedure	Relative density (%)[a]
LNF	1350 °C, 5 h	90
LSFMC	1250 °C, 10 h	98
LNC	1200 °C, 5 h	79
LSF	1150 °C, 5 h	93

[a] Theoretical density was calculated from the results obtained in Rietveld analysis. Experimental density was determinated geometrically from the volume and weight of the samples.

oxygen reduction reaction in the cathode triple-phase boundaries has more electrons from the interconnect, resulting in a substantial increase in cell performance. It was also found that cell degradation inside the stack, is principally dependent on the interfacial contact between the cathode current collecting layer and the interconnect [7].

The cathode contact material composition is required to possess high electrical conductivity and appropriate sintering activity to minimize the resistance of the contact layer itself and to protect the steel substrate from excessive oxidation. Besides, it must be chemically compatible with both the protective materials or chromia-forming interconnects and the perovskite cathodes. The contact material, as well as, its reaction products should demonstrate an appropriate thermal expansion behavior and high thermochemical and structural stability in the oxidizing cathode environment [8,9].

Cathode/interconnect contact materials in SOFCs include many type of compounds: i) noble metals (Ag) or noble metal–perovskite composites (Ag-$(La_{0.6}Sr_{0.4})(Co_{0.8}Fe_{0.2})O_3$, Ag–$La_{0.8}Sr_{0.2}MnO_3$), ii) conventional perovskite cathode materials [10] (such as, $La_{0.8}Sr_{0.2}Co_{0.75}Fe_{0.25}O_3$, $La_{0.8}Sr_{0.2}FeO_3$), iii) oxides with a spinel structure, M_3O_4 (M = Ni, Mn, Co, Cu, Fe), or iv) recently developed oxides like $Ni_{0.33}Co_{0.67}O$. Despite the interactions of these kind of materials with Cr-containing steel interconnects, due to their susceptibility to form phases like Ag_2CrO_4, $AgCrO_2$, $SrCrO_4$, Cr-spinels or Cr-perovskites, the use of those materials, in most of the cases, are quite effective for improving the electrical contact between the cathodes and metallic interconnects [11–15]. In this study, $(La_{0.8}Sr_{0.2})_{0.95}Fe_{0.6}Mn_{0.3}Co_{0.1}O_3$ (LSFMC), $LaNi_{0.6}Fe_{0.4}O_{3-\delta}$ (LNF) and $LaNi_{0.6}Co_{0.4}O_{3-\delta}$ (LNC) were selected for their use as contact layers, for intermediate cell operation temperature (IT-SOFC, 600–800 °C), due to their adequate sintering activity, electrical conductivity and thermal expansion coefficient (TEC). To carry out this study, lanthanum strontium ferrite, $La_{0.6}Sr_{0.4}FeO_3$ (LSF), has been chosen as cathode due to its acceptable electric and ionic conductivity, relative control of the porosity and enough catalytic activity that allows the reduction of the oxidant gas (air or oxygen) at low operating temperatures [16]. As interconnect Crofer22APU was selected due to its good workability, high corrosion resistance and cost-effectiveness [17].

In the present research, three perovskites, LSFMC, LNF and LNC were investigated as contact materials. Phase structure using XRD, electrical conductivity and TEC values of selected materials were determinated. Results of electrical performance and chemical stability of cathode contact materials in combination with Crofer22-APU and $La_{0.6}Sr_{0.4}FeO_3$ as interconnect and cathode, respectively, are presented and discussed. In addition, the system {steel/LSF/LSF} without a contact layer was also studied for comparison. The use of different perovskites as contact materials based on its properties and, on contacting resistance and chemical compatibility of each system will be discussed.

2. Experimental

Powders of $(La_{0.8}Sr_{0.2})_{0.95}Fe_{0.6}Mn_{0.3}Co_{0.1}O_3$ (LSFMC), $LaNi_{0.6}Fe_{0.4}O_{3-\delta}$ (LNF), $LaNi_{0.6}Co_{0.4}O_{3-\delta}$ (LNC) and $La_{0.6}Sr_{0.4}FeO_3$ (LSF) were purchased from NexTech, Fuel Cell Materials, and Crofer22APU was obtained from ThyssenKrupp VDM. X-ray Diffraction (XRD) at room temperature, using a Philips X'Pert PRO diffractometer equipped with Cu K_α radiation ($\lambda = 1.5418$ Å), was used to check phase structures of the commercial materials. The power generator has been provided at 40 kV and 40 mA. The patterns were recorded in 2θ steps of 0.026° in the 18–90° range. The diffraction data of the samples were fitted in all the cases by Rietveld method using the FULLPROF program [18–20].

For bulk conductivity and TEC measurements, pellets of powders were sintered at the temperatures shown in Table 1 to achieve full density. Then, sintered pellets were cut in ~1 × 3 × 7 mm bars; the conductivity measurements were carried out with the standard dc four-point method on the rectangular sintered bars, from room temperature to 1000 °C in air with a heating rate of 2 °C min^{-1}, using a power source controlled by PC using Lab Windows/CVI field point system. The measured conductivity values were corrected taking into account the porosity of the samples [21]. Thermal expansion measurements (TEC) for the contact layers, cathode and interconnect were carried out from room temperature to 1000 °C in air with a heating rate of 5 °C min^{-1} by using a Unitherm Model 1161 dilatometer.

The contact evaluation of the studied material layers between Crofer22APU interconnect and LSF cathode was carried out with the interconnect preoxidized at 800 °C for 100 h in air in a Carbolite furnace. Prior to the oxidation, the sheets were cut into 10 × 10 mm

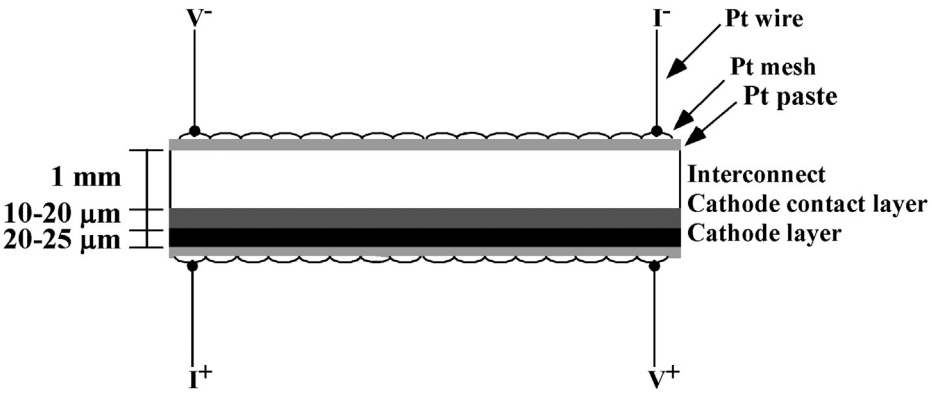

Fig. 1. Sample setup for contact ASR measurement of {Crofer22APU/contact layer/LSF} system.

Table 2
Main emission lines for the analyzed elements.

Element	K_α (keV)	K_β (keV)	L_α (keV)	L_β (keV)
La			4.650	5.041
Cr	5.411	5.946		
Mn	5.894	6.489		
Fe	6.398	7.057		
Co	6.924	7.648		
Ni	7.471	8.263		

squares with 1 mm thickness, and also were polished using #800 grit SiC, cleaned with acetone in an ultrasonic bath and dried. As observed in other studies, preoxidation of interconnect may reduce Cr and Fe transport into the contact coating, after long oxidation times. In addition, preoxidized samples developed thin coating which may decrease interfacial stress over time between the contact layer and interconnect [22]. The deposition of the contact materials was carried out using wet colloidal spray deposition technique, as was described in Refs. [23], and sintered at 1050 °C for 2 h to obtain a rather dense coating. LSF cathode was deposited on contact layers using the same deposition technique and sintered at 950 °C for 2 h to produce a porous layer. The suspensions were made mixing in a ball mill during 1 h the powders, ethanol and ZrO_2 cylinders as grinding media. For the area specific resistance (ASR) measurements a dc four-point method was used and, samples were prepared according to the geometries shown in Fig. 1. Electrical contact between the sandwich structure and external measuring circuit were obtained with two Pt wires welded to the Pt mesh at interconnect and cathode side, in combination with Pt paste onto the surface of interconnect and cathode. The overall ASR of {Crofer22APU/contact material/cathode} setup was measured at 800 °C for up to 16 h to evaluate the starting point stability of the obtained contact resistance values, and it was estimated by the voltage value measured by chronoamperometry applying a current of 300 mA, using a VSP Potentiostat/Galvanostat (Princeton Applied Research, Oak Ridge, US). Cross-section of the sandwich structures, after contact resistance measurements, were then metallographically prepared and investigated with scanning electron microscope (SEM, JEOL LSM-6400) equipped with an Oxford Pentafet energy dispersive X-ray analyzer (EDX) to study the microstructure of the systems and, to determinate extend of interdiffusion between materials. The composition analysis on the samples cross-section was made using back-scattered electrons (BSE) at 20 kV accelerating voltage, $1{\cdot}10^{-9}$ A current density and 15 mm working distance. Due to the overlap of the emission lines for the studied

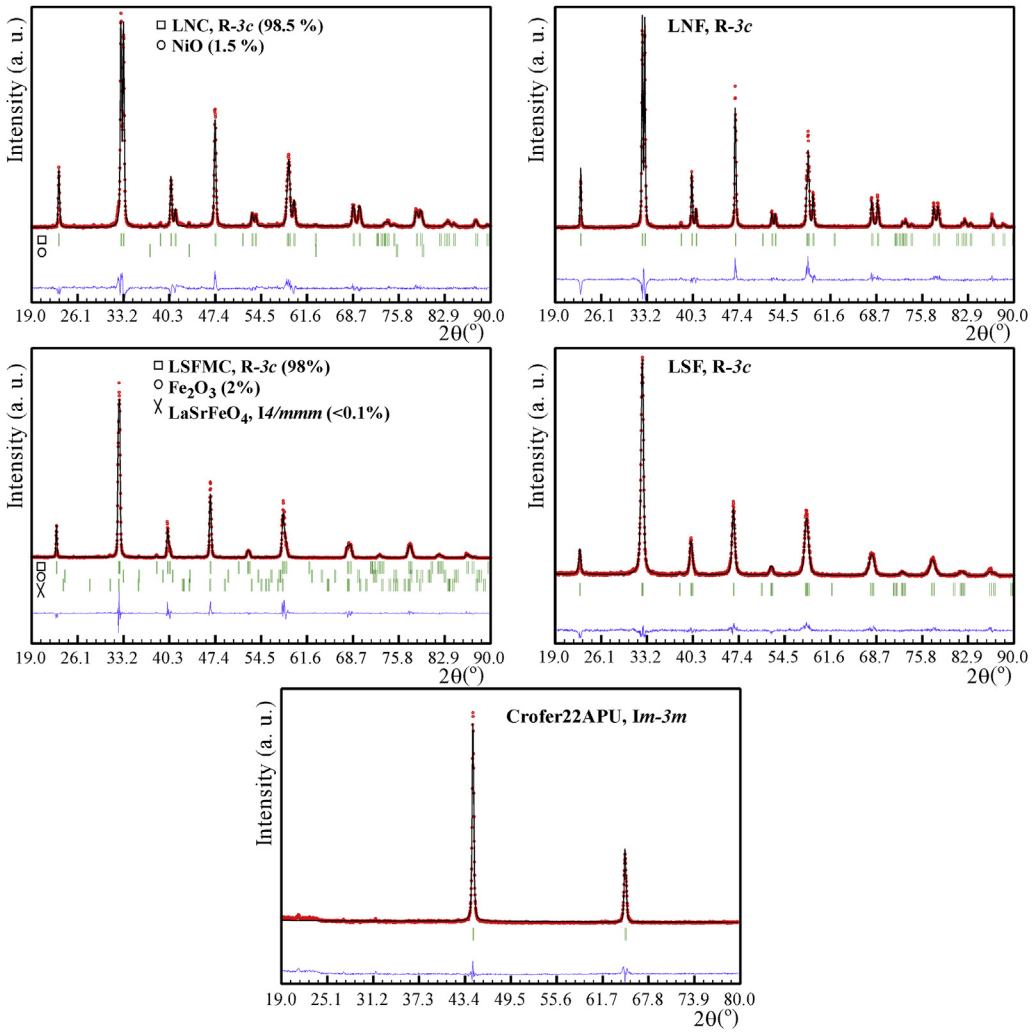

Fig. 2. Rietveld X-ray diffraction pattern refinements for commercial LSF, LSFMC, LNF, LNC and Crofer22APU materials. Circles denote experimental points; upper solid line the calculated profile. Theoretical peak positions (vertical sticks) and difference lines are shown in the bottom of each pattern.

Table 3
General structural parameters obtained from the Rietveld analysis.

Material	Space group	Lattice parameters a (Å)/c (Å)	V (Å^3)	χ^2
LNC	R-3*c*	5.459(1)/13.137(1)	339.04(1)	3.29
LNF	R-3*c*	5.513(1)/13.272(1)	349.33(1)	3.77
LSFMC	R-3*c*	5.522(1)/13.412(1)	354.22(1)	3.33
LSF	R-3*c*	5.528(1)/13.451(2)	355.93(1)	2.03
Crofer22APU	I*m*-3*m*	2.881(1)	23.91(1)	7.31

elements (Table 2), the INCA 350 software from Oxford was used to reconstruct the spectra and it was compared with the measured one to confirm the presence or absence of these elements.

3. Results and discussion

3.1. Phase characterization

The phase structures of studied commercial materials (LNC, LNF, LSFMC, LSF and Crofer22APU) were refined by the Rietveld method, as shown in Fig. 2. All the perovskite phases showed a rhombohedral structure with R-3*c* space group; however, steel has a cubic arrangement and it crystallizes in space group I*m*-3*m*, as expected. The refined cell parameters and unit cell volumes are summarized in Table 3. The quantitative analysis demonstrates that the studied materials were pure except LSFMC and LNC. For LNC two very weak peaks corresponding to NiO were found (1.5% in weight) and for LSFMC, Fe_2O_3 phase (2% in weight) and traces of $LaSrFeO_4$ (<0.1% in weight) were quantified.

The dependence of conductivity of each perovskite on temperature and the Arrhenius plot for the electrical conductivity in air is shown in Figs. 3 and 4, respectively. The conductivity increases with increasing temperature up to a maximum and then decreases due to the lattice oxygen loss, for the LSFMC, LSF and LNF perovskites, implying a small semiconductor behavior [21]. For the LNC material, however, the conductivity decreases continuously with increasing temperature, implying a metallic behavior [24].

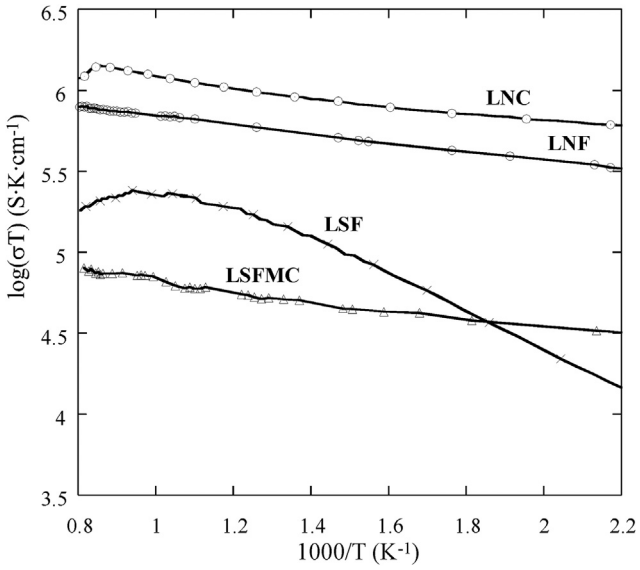

Fig. 4. Arrhenius plot of selected perovskites as a function of temperature.

For the compositions with semiconducting behavior, the temperature dependence of the conductivity can be described by the small polaron hopping mechanism [25] as it shown in Equation (1):

$$\sigma = \frac{A}{T}\exp\left(\frac{-Ea}{KT}\right) \quad (1)$$

where A is the pre-exponential factor, T is the temperature, k is the Boltzmann constant, and Ea is the activation energy for the hopping

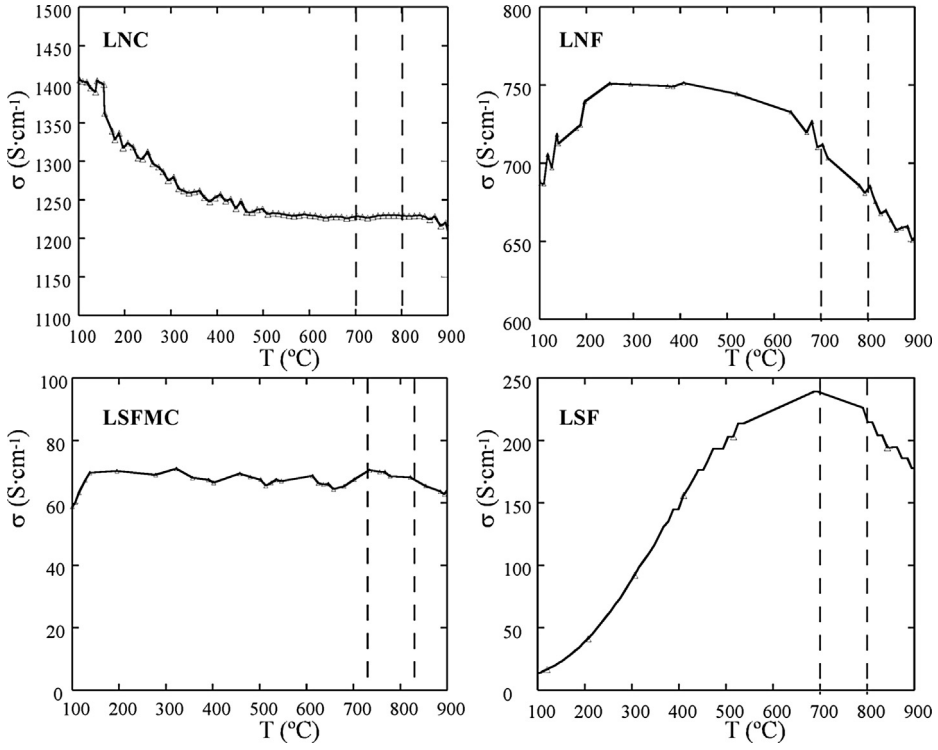

Fig. 3. Electrical conductivity of $(La_{0.8}Sr_{0.2})_{0.95}Fe_{0.6}Mn_{0.3}Co_{0.1}O_3$, $LaNi_{0.6}Fe_{0.4}O_{3-\delta}$, $LaNi_{0.6}Co_{0.4}O_{3-\delta}$ and $La_{0.6}Sr_{0.4}FeO_3$ perovskites as a function of temperature.

Table 4
Maxima in conductivity, conductivity values at 800 °C and activation energy obtained from the Arrhenius plots for all the compounds.

Composition	σ_{Max} (S cm^{-1}), T_{Max} (°C)	$\sigma_{800\,°C}$ (S cm^{-1})	E_a ($RT - T_{Max}$) (eV)
$LaNi_{0.6}Co_{0.4}O_{3-\delta}$ (LNC)[a]	1405.9	1229	–
$LaNi_{0.6}Fe_{0.4}O_{3-\delta}$ (LNF)	751.4	685	0.02
$(La_{0.8}Sr_{0.2})_{0.95}Fe_{0.6}Mn_{0.3}Co_{0.1}O_3$ (LSFMC)	71.3	65	0.08
$La_{0.6}Sr_{0.4}FeO_3$ (LSF)	239.7	214	0.11

[a] For LNC sample the activation energy was not calculated due to it exhibit metallic electrical conduction in every range of temperature.

of the small polarons. The activation energy obtained from the Arrhenius plots (for LSFMC, LSF and LNF samples) and the maximum in conductivity and at 800 °C for all compounds are given in Table 4.

The obtained conductivity values of the samples are in good agreement with other studies for these types of compounds [14,26–29]. As observed, at 800 °C the LNC and LNF show higher conductivity than LSFMC, whose conductivity value is smaller than the one obtained for the cathode material (LSF). It is known that conductivity of contact materials is one of the most important properties for ensuring acceptable ASR. However, the selection of contact material also depends on mechanical integrity of the Crofer22APU/contact layer/LSF interfaces and on its stability. Thus, in terms of conductivity LNF and LNC are appropriate to use as contact layer and, LSFMC is a suitable choice according to its mechanical integrity [3] and also because its TEC value is closely matched with that of the interconnect, as shown below.

Fig. 5 shows the thermal expansion curves of the five materials obtained upon heating from 200 to 1000 °C. The TEC results present close to linear dependence in the temperature range of 30–1000 °C for the Crofer22APU and LNC samples. For the other materials, however, the curves become steeper above the temperature at which each compound shows the maximum in conductivity, corresponding probably to a lattice oxygen loss giving rice to the lattice expansion. As it has been discussed in other works [29–31], this lattice expansion, associated with the formation of oxygen vacancies, can be attributed to: a) the repulsion force arised between those mutually exposed cations when oxygen ions are extracted from the lattice; and/or b) the increase in cation size due to the

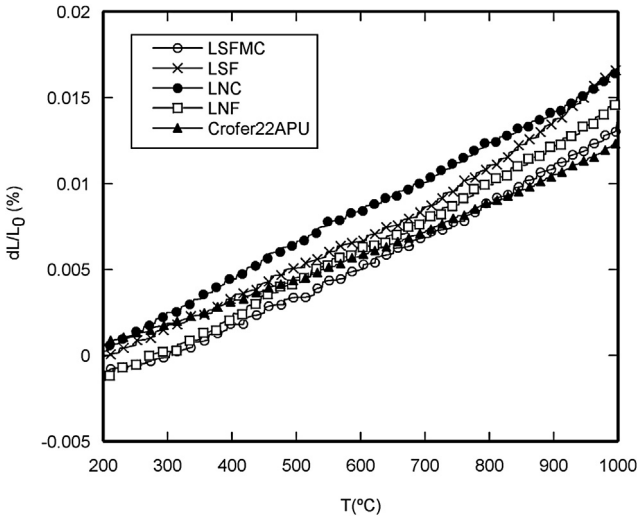

Fig. 5. Thermal expansion curves of the materials that compose the studied systems, obtained upon heating from 200 to 1000 °C in air.

Table 5
Thermal expansion coefficients for the studied materials.

Component	Material	$\alpha_{30-800\,°C}$ (K^{-1})	$\alpha_{30-1000\,°C}$ (K^{-1})
Interconnect	Crofer22APU	$11.8\cdot10^{-6}$	$12.8\cdot10^{-6}$
Contact layer	LNC	$17.9\cdot10^{-6}$	$17.5\cdot10^{-6}$
Contact layer	LNF	$16.1\cdot10^{-6}$	$16.0\cdot10^{-6}$
Contact layer	LSFMC	$14.5\cdot10^{-6}$	$14.6\cdot10^{-6}$
Cathode	LSF	$16.1\cdot10^{-6}$	$17.5\cdot10^{-6}$

reduction of Co and Fe ions from higher to lower valences, which must occur concurrently with the formation of oxygen vacancies in order to maintain the electrical neutrality.

The average TECs at different temperatures for all the components studied are listed in Table 5. As expected, Co based perovskite shows higher TEC values than obtained for Co-free perovskites, such as manganites, nickelites and ferrites [32–35]. As can be observed, for LNF and LNC, the $\alpha_{30-800\,°C}$ and $\alpha_{30-1000\,°C}$ values are comparables to those obtained for the cathode, respectively. For LSFMC, however, these TEC values are smaller showing intermediate values between LSF cathode and Crofer22APU interconnect. The measured average TECs are higher than the ones reported in other works [16,36–38] for this type of compositions. Those small differences can be attributed to the influence of the sample preparation method and different sintering temperatures [39].

The TEC values obtained for the interconnect material is smaller than for the other components of the cell, especially for the LNC and LNF compositions. Although the TEC values are not exactly the same, they present an obvious concern for integrity of the contact layers and interfaces during thermal cycling. It is necessary to remark that for the cell preparation, the contact layer will be relatively thin with a certain porosity to ensure the flow of oxygen, properties that are expected to reduce thermal stress. In the preparation of the cells, all of these materials have been successfully employed as contact layer between cathode and interconnect, despite having larger TEC than Crofer22APU material.

From these results, it can be concluded that: a) LNC and LNF compounds present the highest conductivity values and their TECs values are comparables to those obtained for the cathode and, b) despite the fact that LSFMC showed the lowest conductivity, the TEC results obtained for this perovskite presents the best fit with the TEC values obtained for the interconnect.

3.2. ASR measurements and post-test analysis

Fig. 6 shows that ASR values (Table 6) of the different contact perovskites tested are stable during the contact resistance

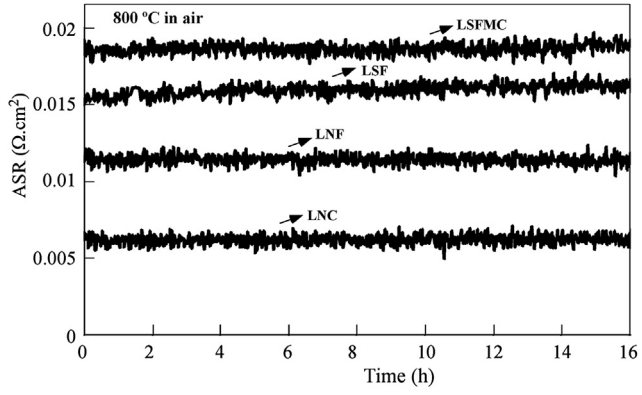

Fig. 6. ASR for {Crofer22APU/contact layer/LSF} interfaces as a function of time with different contact materials and for the {Crofer22APU/LSF/LSF} system.

Table 6
Area specific resistance values for the different tested contact perovskites measured at 800 °C in air.

System: Crofer22APU/contact layer/LSF	≈ ASR (Ω cm^2)
LNC	0.006(1)
LNF	0.010(1)
LSF	0.015(1)
LSFMC	0.018(1)

measurements. The contact made by LNC, which has the lowest electrical resistance among the three selected perovskites, gives the lowest ASR, while the contact made by LSFMC, which present a lower electrical conductivity, leads to a higher contact resistance. The value of the electrical resistance for the system with only LSF amounts to 0.015 Ω cm^2, and it was relatively constant during the experiment. The ASR values for the systems with the LNC and LNF contact layers are 0.006 and 0.010 Ω cm^2, respectively. These values are lower than that for the system with LSF only, as was expected for LSFMC this value is higher and amounts to 0.018 Ω cm^2. The achieved contact resistance values are considerably lower than that of previously reported results for this kind of materials [3]. However, it has been published for {interconnect: AISI441/contact layer: $Ni_{0.33}Co_{0.67}O$/cathode: $La_{0.8}Sr_{0.2}MnO_3$} combination and for {interconnect: 441SS/protective coating: $Mn_{1.5}Co_{1.5}O_4$/contact layer: $La_{0.7}Sr_{0.3}CoO_3$/cathode: $La_{0.6}Sr_{0.4}Co_{0.8}Fe_{0.2}O_3$} assemblies the same order of ASR values [2,12]. The significantly low ASR was probably due to the microstructure and thickness of the different layers, and/or due to the good bonding of the interfaces between contact layer and cathode, and contact layer and interconnect. It is known [40] for this kind of systems that the initial area specific resistance mainly depends on electrical conductivity of the measured perovskites while the time evolution of the ASR depends on the interactions between the contact materials and adjacent components. For this reason it is difficult to assert that the reaction products between ferritic steel and contact or cathode layers exhibit sufficiently high electronic conductivity not to increasing the contact resistance.

The polished cross-sections of different systems after ASR measurements at 800 °C are shown in Fig. 7. Five layers can be distinguished in all the samples, including: the interconnect, the oxide scale, the contact layer, the cathode and the Pt paste. The thicknesses of the contact materials can be estimated to be between 10 and 20 μm, respectively. In addition, in all cases, the thickness of the cathode is about 20–25 μm. The total thickness of the oxide scale for the combination with LSFMC is similar to the system with LNF, which is about 1.5 μm. The oxide layers formed at the LNC/and LSF/Crofer22APU interfaces are not completely homogeneous in thickness. It is likely that the protective chromia scale growth rate, depends on the contact material composition. This effect can be also related to the amount and distribution of minor alloying additions in Crofer22APU, such as reduction of Si and Al additives, leading to an increase of oxidation rates during the preoxidation of the interconnect [41].

The microstructure of the cathode layer in all the samples is similar, revealing open porosity with a pore size of approximately 0.5–2 μm. The pore size distribution of the contact pastes depends on the reactivity undergone by each system after ASR measurements. The pores over the contact layer cross-sections for LNF, LNC and LSFMC have a diameter of about 1 μm, whereas for LSF is about 0.5–1 μm. Compared to other three contact materials, LSF has fewer pores and it shows a quite uniform distribution of the pores. In all the samples the contact layers were well bonded to the metallic substrate. However, during the preoxidation process of

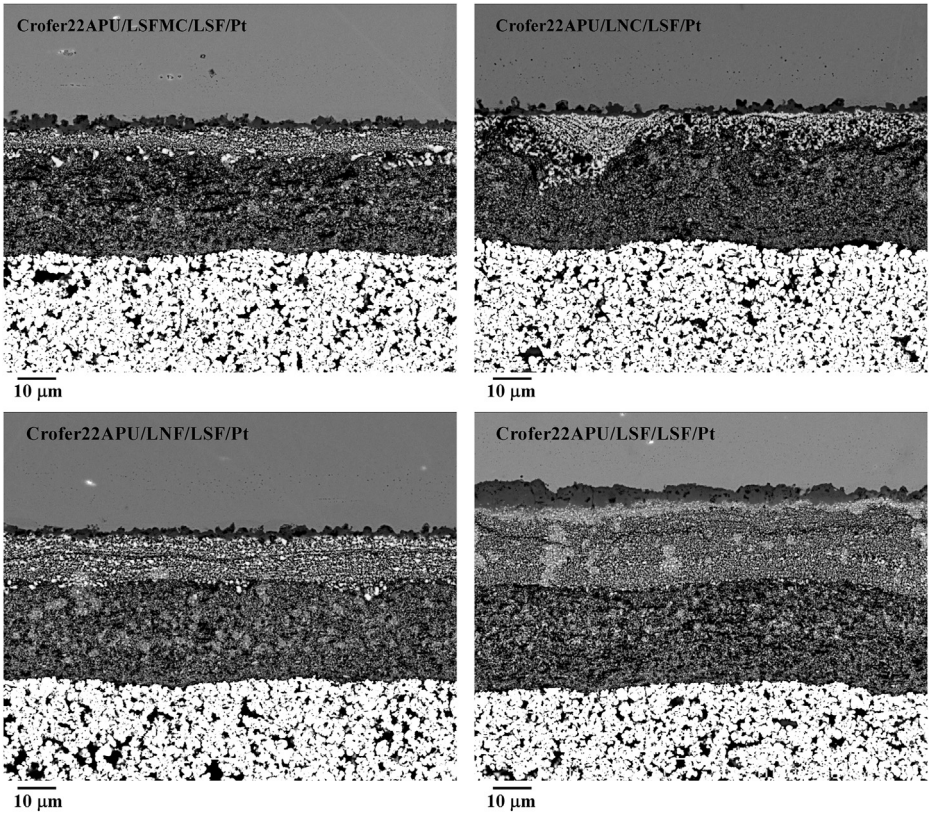

Fig. 7. Metallographic cross-sections (back-scattered electron image) of the different {Crofer22APU/contact layer/LSF} systems after ASR measurements at 800 °C in air.

the interconnect, the formation of voids at the interface between the oxide scale and the steel can be detected. According to other studies [41] insufficient La in the steel melt can lead to void formation. The cathode and contact layer are well attached especially when LSF was used as contact material and also for LNF combination. For LNC and LSFMC systems the cathode is not so properly attached to the contact layer, probably due to the mismatch between TECs values.

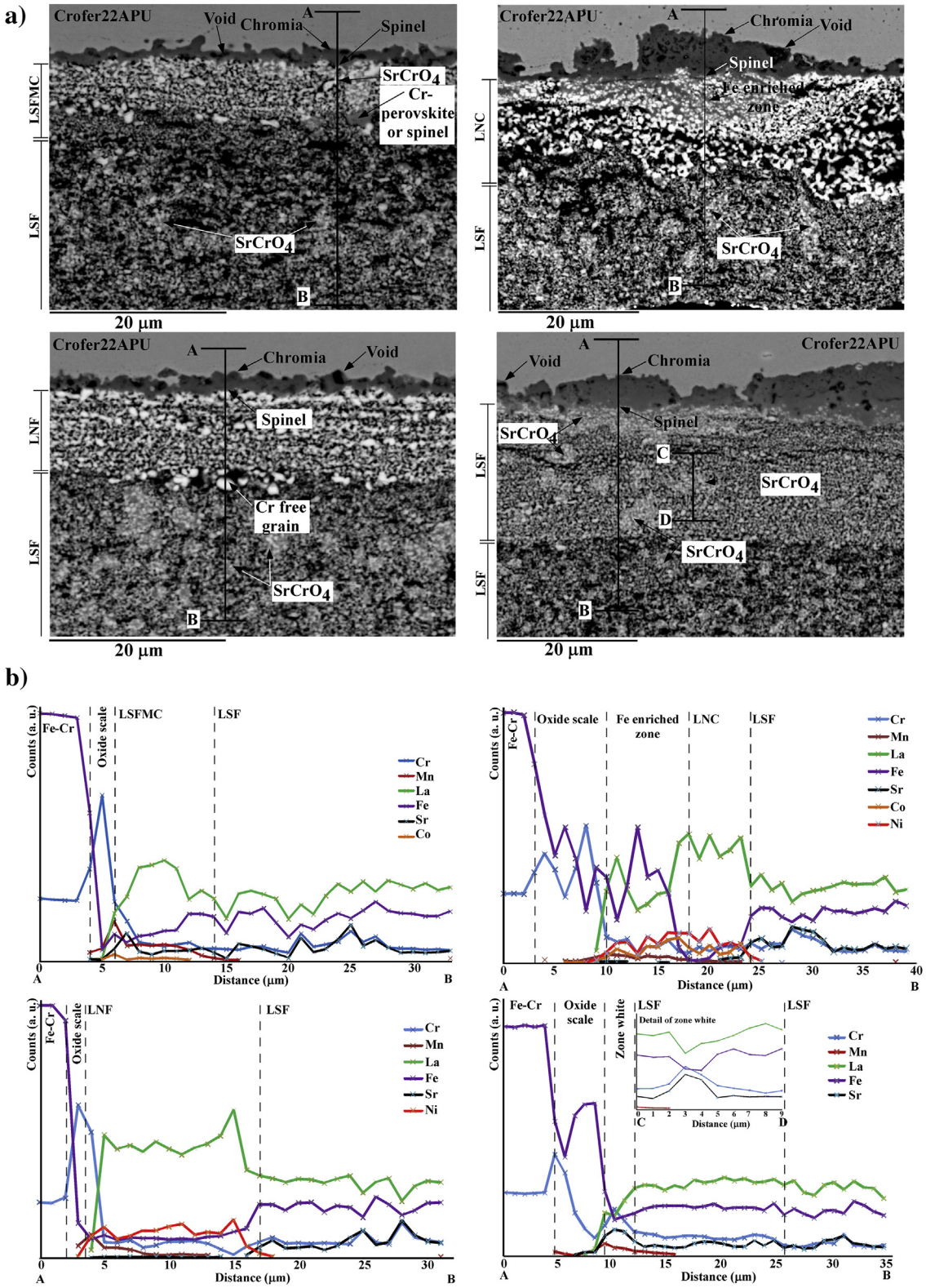

Fig. 8. a) Details of SEM cross-sections of studied systems after contact resistance measurements, b) representative results to estimate the extent of interdiffusion at the different systems interfaces from EDX point analysis.

To estimate the extent of interfacial interdiffusion, in the starting hours, for the contact material and the interconnect, or the contact material and the cathode, linescans were performed using EDX analysis along the samples as shown in Fig. 8. For all the cases, oxide scale is composed of two layers: Cr_2O_3 bonded to the metal substrate followed by $(B)_3O_4$ spinel layer (B = Cr, Co, Fe, Ni, Mn) in good agreement with the literature [42]. The growth of chromia is governed by an outward and inward diffusion of Cr and O, respectively [43].

The addition of manganese as additive in the alloy enhances the formation of the spinel formed under the Cr_2O_3 layer and, it improves the scale conductivity which prevents chromium migration and formation of Cr(VI) oxide and oxy-hydroxide species. Thus, the reduction in the rate of cathode degradation by Cr poisoning is

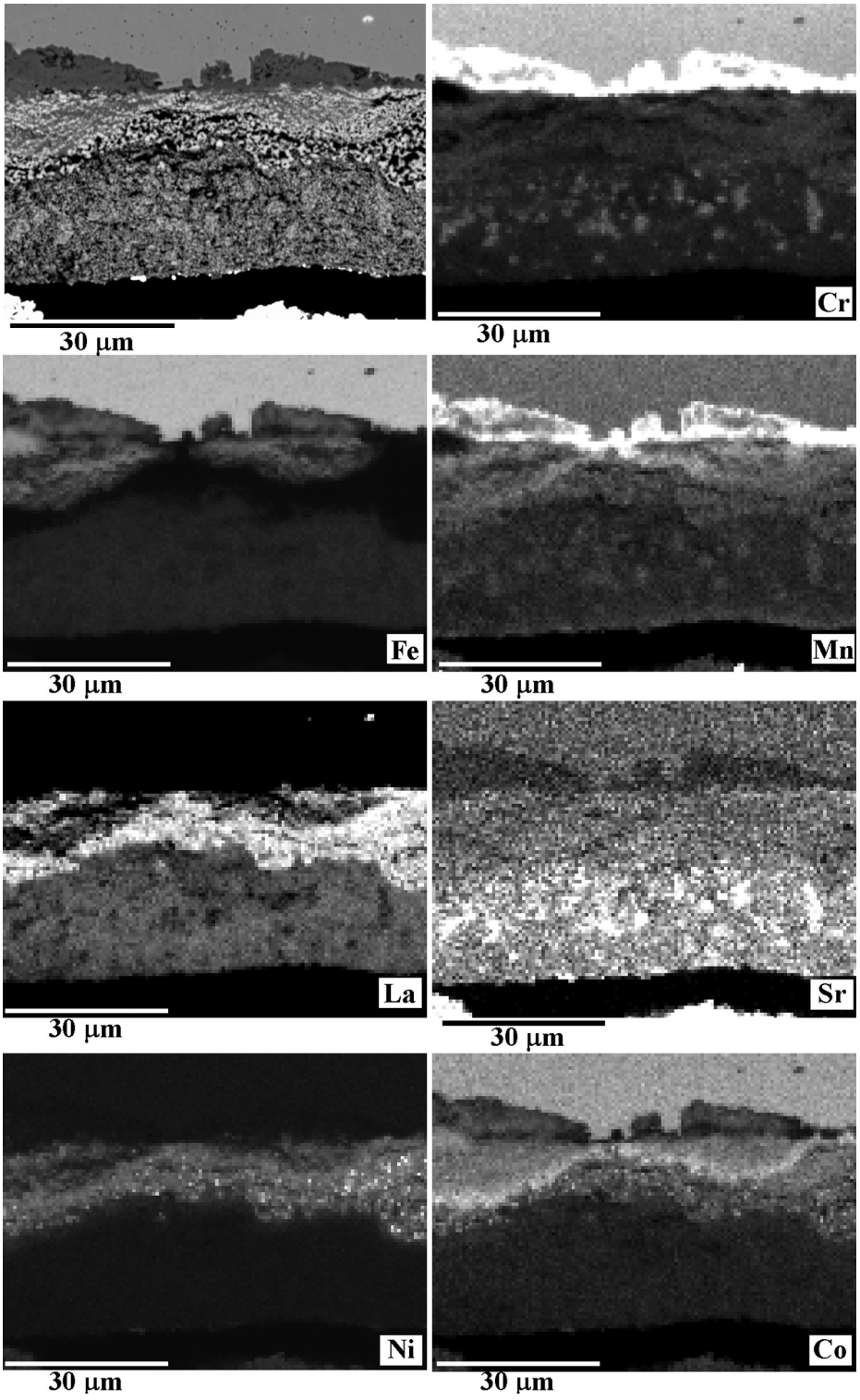

Fig. 9. EDX mapping of the cross-section of {Crofer22APU/LNC/LSF} combination after ASR measurements in air at 800 °C.

given. Therefore, Mn-containing perovskites like LSFMC can also facilitate the formation of Cr–Mn spinels. For Co- and Fe-containing perovskites, such as LNC and LNF, the cobalt and iron released from the perovskite lattice can react with the Cr and Mn from the oxide scale to form $(Cr, Mn, Co, Fe)_3O_4$ spinels. The existence of Fe or Co ions in the spinel grains might improve considerably the electrical conductivity of the coated sample.

For all the systems, the element interdiffusion between cell components is mainly concentrated on Fe, Cr and Mn which released from the interconnect. In the cross-section imagenes gray colored zones can be detected within the contact and cathode material probably associated to the formation of Cr-containing perovskites [44–46]. The presence of some cracks through the ceramic layers, specially observed for LNC, and the chromium enrichment zones observed for all the systems, can contribute to a higher densification of coating causing in some of the systems cracks. In addition, the cracks can be explained by interactions between contact material and oxide scale, leading to expanded volume of the layer.

Due to the mobility of Sr in cathode environment, large regions enriched with Cr and Sr are observed within the LSF and LSFMC layers owing to $SrCrO_4$ precipitation [47], which is detected [3] as "white zones" in the images.

When LNC contact material is used, a Fe enriched zone with many different compositions was formed between chromia scale and LNC coating (Fig. 9). Considering that denser contact layer retains better Cr, it can be deduced that a decrease in the degree of compaction of the layer makes increasing in chromia evaporation, thereby leading to the low concentration of Cr_2O_3 in Crofer22APU/LNC interface. Thus, the increase in the concentration of Fe oxides like Fe_2O_3 is given. This oxide is less dense than Cr_2O_3 and may facilitate cation diffusion of Cr^{3+}, Mn^{3+} and Fe^{3+} to the surface, resulting in a reaction with the contact coating [48]. Despite the open porosity of the contact layer, LNC gives the lower ASR due to its higher conductivity.

4. Conclusions

Direct contact between interconnect and cathode in IT-SOFC stack generally leads to electrical losses. They can be diminished by appropriate contact layers. Three lanthanum-based perovskite ceramic compounds, $(La_{0.8}Sr_{0.2})_{0.95}Fe_{0.6}Mn_{0.3}Co_{0.1}O_3$ (LSFMC), $LaNi_{0.6}Fe_{0.4}O_{3-\delta}$ (LNF) and $LaNi_{0.6}Co_{0.4}O_{3-\delta}$ (LNC) were selected as contact materials for this study. The observed high conductivity values for LNF and LNC and, the good fit between TECs values of LSFMC and the interconnect make the use of these materials as contact layers interesting.

The thickness of oxide scale observed for the combination with LSFMC and LNF is reasonable homogeneous in contrast with systems with LNC and LSF in which this oxide scale is not uniform. This effect can be related to the distribution of minor additives within interconnect which produces differences in scale growth or, it can be also associated to the contact material compositions. For all cases, oxide scale is composed of two layers: Cr_2O_3 bonded to the metal substrate followed by spinel layer. The Mn-, Co- and Fe-containing perovskites used in this study lead to the formation of spinels with different compositions which can improve electrical conductivity of coated samples. In the four systems the chromium enrichment observed in contact and cathode layers allowed the formation of phases like $SrCrO_4$ and Cr-containing perovskite in short exposure times. When LNC contact material is used, a Fe enriched zone with many different compositions is formed between chromia scale and contact coating probably due to the open porosity of the contact layer which prevents the formation of protective coating of chromia. The obtained contact resistance values are strongly influenced by the conductivity of the selected contact material. The ASR contribution of all the systems is fairly acceptable for the performance of a SOFC stack operating in the intermediate temperature range.

The selection of the best contact layer is based on a compromise between mechanical integrity of the Crofer22APU/contact layer/LSF interfaces and, contact resistance and chemical compatibility of the system. In the present case, LNF coating can be a suitable choice as contact coating due to the adequate integrity and low reactivity between the applied layers without compromising the contact resistance of the system. Future work will include long-term stability of {Crofer22APU/LNF/LSF} system in terms of contact resistance and chemical compatibility.

Acknowledgment

This research has been funded by the Consejería de Industria, Innovación, Comercio y Turismo (SAIOTEK 2012 programmes), by Dpto. Educación, Política Lingüística y Cultura of the Basque Goverment (IT-630-13) and by Ministerio de Ciencia e Innovación (MAT2010-15375 and MAT2012-30763). The authors thank Ikerlan's Fuel Cell group and SGIker technical support (UPV/EHU, MEC, GV/EJ and European Social Fund). A. Morán-Ruiz thanks UPV/EHU for funding her PhD work.

Appendix A. Supplementary data

Supplementary data related to this article can be found at http://dx.doi.org/10.1016/j.jpowsour.2013.10.031.

References

[1] S.P. Jiang, J. Electrochem. Soc. 148 (8) (2001) A887.
[2] M.C. Tucker, L. Cheng, L.C. Dejonghe, J. Power Sources 196 (2011) 8313.
[3] X. Montero, F. Tietz, D. Stöver, M. Cassir, I. Villarreal, J. Power Sources 188 (2009) 148.
[4] M.C. Tucker, L. Cheng, L.C. DeJonghe, J. Power Sources 224 (2013) 174.
[5] Y. Tao, H. Nishino, S. Ashidate, H. Kokubo, M. Watanabe, H. Uchida, Electrochim. Acta 54 (2009) 3309.
[6] W.B. Guan, H.J. Zhai, L. Jin, T.S. Li, W.G. Wang, Fuel Cells 3 (2011) 445.
[7] W.B. Guan, L. Jin, X. Ma, W.G. Wang, Fuel Cells 6 (2012) 1085.
[8] Z. Yang, G. Xia, P. Singh, J.W. Stevenson, J. Power Sources 155 (2006) 246.
[9] B.P. McCarthy, L.R. Pederson, Y.S. Chou, X.D. Zhou, W.A. Surdoval, L.C. Wilson, J. Power Sources 180 (2008) 294.
[10] S.J. Skinner, M.A. Laguna-Bercero, in: D.W. Bruce, D. O'Hare, R.I. Walton (Eds.), Energy Materials, John Wiley & Sons, Ltd, Chichester, UK, 2011, http://dx.doi.org/10.1002/9780470977798.ch2.
[11] L.T. Wilkinson, J.H. Zhu, J. Electrochem. Soc. 156 (8) (2009) B905.
[12] Z. Lu, G. Xia, J.D. Templeton, X. Li, Z. Nie, Z. Yang, J.W. Stevenson, Electrochem. Commun. 13 (2011) 642.
[13] M.T. Tucker, L. Cheng, L.C. Dejonghe, J. Power Sources 196 (2011) 8435.
[14] F. Wang, D. Yan, W. Zhang, B. Chi, J. Pu, L. Jian, Int. J. Hydrogen Energy 38 (2013) 646.
[15] W. Zhang, F. Wang, K. Wang, J. Pu, B. Chi, L. Jian, Int. J. Hydrogen Energy 37 (2012) 17253.
[16] U.F. Vogt, P. Holtappels, J. Sfeir, J. Richter, S. Duval, D. Wiedenmann, A. Züttel, Fuel Cells 6 (2009) 899.
[17] V. Miguel-Perez, A. Martínez-Amesti, M.L. Nó, A. Larrañaga, M.I. Arriortua, Corros. Sci. 60 (2012) 38.
[18] H.M. Rietveld, J. Appl. Crystallogr. 2 (1969) 65.
[19] J. Rodríguez-Carvajal, Phys. B 192 (1993) 55.
[20] J. Rodríguez-Carvajal, FULLPROF Rietveld Pattern Matching Analysis of Powder Patterns, 1994. Grenoble.
[21] K. Vidal, L.M. Rodríguez-Martínez, L. Ortega-San-Martín, M.L. Nó, T. Rojo, M.I. Arriortua, Fuel Cells 11 (2011) 51.
[22] K.O. Hoyt, P.E. Gannon, P. White, R. Tortop, B.J. Ellingwood, H. Khoshuei, Int. J. Hydrogen Energy 37 (2012) 518.
[23] A. Martínez-Amesti, Celdas de Combustible de Óxido Sólido. Estudios de Reactividad y Optimización de la Intercapa Cátodo-Electrolito (Ph. D. thesis), UPV/EHU, 2009.
[24] A. Huang, K. Yao, J. Wang, J. Electroceram. 16 (2006) 313.
[25] P.A. Cox, The Electronic Structure and Chemistry of Solids, Oxford Science Publications, Oxford, UK, 1987.
[26] K. Huang, H.Y. Lee, J.B. Goodenough, J. Electrochem. Soc. 145 (9) (1998) 3220.

[27] M. Bevilacqua, T. Montini, C. Tavagnacco, G. Vicario, P. Fornasiero, M. Graziani, Solid State Ionics 177 (2006) 2957.
[28] H. Ullmann, N. Trofimenko, F. Tietz, D. Stöver, A. Ahmad-khanlou, Solid State Ionics 138 (2008) 79.
[29] J.M. Ralph, J.A. Kilner, B.C.H. Steele, Mater. Res. Soc. Symp. Proc. 575 (2001) 309.
[30] S. Li, Z. Lü, X. Huang, W. Su, Solid State Ionics 178 (2008) 1853.
[31] Z. Li, B. Wei, Z. Lü, X. Huang, W. Su, Solid State Ionics 207 (2012) 38.
[32] Z. Gao, Z. Mao, C. Wang, Z. Liu, Int. J. Hydrogen Energy 35 (2010) 12905.
[33] H. Lv, B.-Y. Zhao, Y.-J. Wu, G. Sun, G. Chen, K.-A. Hu, Int. Mater. Res. Bull. 42 (12) (2007) 1999.
[34] K.T. Lee, A. Manthiram, J. Power Sources 158 (2006) 1202.
[35] H. Taguchi, T. Komatsu, R. Chiba, K. Nozawa, H. Orui, H. Arai, Solid State Ionics 182 (2011) 127.
[36] N. Sukpirom, S. Iamsaard, S. Charojrochkul, J. Yeyongchaiwat, J. Mater. Sci. 46 (2011) 6500.
[37] R. Kumar, E. Yi, Y. Hang, C. Myung, Met. Mater. Int. 15 (2009) 1055.
[38] F. Tietz, I.-A. Raj, M. Zahid, D. Stöver, Solid State Ionics 177 (2006) 1753.
[39] A. Dutta, J. Mukhopadhyay, R.N. Basu, J. Eur. Ceram. Soc. 29 (2009) 2003.
[40] W.J. Shong, C.K. Liu, C.Y. Chen, C.C. Peng, H.J. Tu, G.T.K. Fey, R.Y. Lee, H.M. Kao, Mater. Chem. Phys. 127 (2011) 45.
[41] P. Huczkowski, W.J. Quadakkers, Effect of Geometry and Composition of Cr Steels on Oxide Scale Properties Relevant for Interconnector Applications in Solid Oxide Fuel Cells (SOFCs), Forschungszentrum Jülich, 2007.
[42] S. Fontana, S. Chevalier, G. Caboche, Oxid. Met. 78 (2012) 307.
[43] Y. Zhao, Oxidation Behavior of Ferritic Alloys as Interconnect of Solid Oxide Fuel Cell (SOFC) (Ph. D. thesis), Auburn University, 2012.
[44] M.K. Stodolny, B.A. Boukamp, D.H.A. Blank, F.P.F. van Berkela, J. Electrochem. Soc. 158 (2) (2011) B112.
[45] A. Morán-Ruiz, K. Vidal, A. Larrañaga, M.I. Arriortua, Fuel Cells 3 (2013) 398.
[46] S.P.S. Badwal, R. Deller, K. Foger, Y. Ramprakash, J.P. Zhang, Solid State Ionics 99 (1997) 297.
[47] M.R. Ardigò, A. Perron, L. Combemale, O. Heintz, G. Caboche, S. Chevalier, J. Power Sources 196 (2011) 2037.
[48] V. Miguel-Pérez, A. Martínez-Amesti, M.L. Nó, A. Larrañaga, M.I. Arriortua, J. Power Sources 243 (2013) 419.